האגוד הישראלי למכניקה עיונית ושימושית

The Israel Society for Theoretical and Applied Mechanics

ISTAM

An Adhering Organization of the
International Union of Theoretical and Applied Mechanics
(IUTAM: http://www.iutam.net)

ISTAM Annual Symposium

TECHNICAL PROGRAM

9 December 2007

Tel Aviv University

ISTAM Annual Symposium

9 December 2007

TECHNICAL PROGRAM

Location: Rosenblatt Auditorium, Computer and Software Engineering Building, Tel Aviv University

09:30 – 09:50 Registration and coffee

09:50 – 10:00 *Opening:* MB Rubin, Technion, President of ISTAM

This ISTAM annual symposium is in honor of Prof. Kalman Schulgasser

Morning Session Chairman: **R Segev**, Ben-Gurion University.

10:00 – 10:25 **K Schulgasser**, Ben-Gurion University. *Under the Chiral Tree*

10:25 – 10:50 **Y Benveniste** and T Miloh. Tel Aviv University. *Soft neutral elastic inhomogeneities with membrane-type interface conditions*

10:50 – 11:15 **N Trabelsi**, Z Yosibash, S Gruntman, Y Alon and C Milgrom, Ben-Gurion University. *Patient-specific simulation of the proximal femur's mechanical response validated by experimental observations*

11:15 – 11:40 G Jourdan, L Houas and **O Igra**, Ben-Gurion University. *Shock tube study of the drag coefficient of a sphere.*

11:40 – 12:05 **A Gat**, I Frankel and D Weihs, Technion. *Effects of straight-walled constrictions on flow in shallow micro-channels*

ISTAM Society Meeting (Registered members only) Chairman: **E Altus**, Technion

12:05 – 12:30 International Center for Mechanics in Beijing. Election of the President of ISTAM

12:30 – 14:00 Lunch (The registration fee includes lunch)

Afternoon Session Chairman: **L Banks-Sills**, Tel Aviv University.

14:00 – 14:25 **A Rotem**, Technion. *Failure criteria for isotropic and fibrous laminated composite materials - three dimensional loading case*

14:25 – 14:50 M Perl and **V Bernstein**, Ben-Gurion University. *Three-Dimensional Stress Intensity Factors for a Multicracked Spherical Pressure Vessel*

14:50 – 15:15 **D Rittel** and A Brill, Technion. *Dynamic flow and failure of confined polymethylmethacrylate*

15:15 – 15:40 **Y Ganor** and D Shilo, Technion. *Work output enhancement of ferromagnetic shape memory micro actuators*

15:40 – 16:05 **S Yulzary** and D Elata, Technion. *The electromechanical response of a double-axis electrostatic comb-drive actuator*

The annual membership fee to ISTAM is 60 NIS. It includes the lunch at the symposium and can be paid during the registration.

All lectures are open to the public free of charge

Under the Chiral Tree

K Schulgasser

Department of Mechanical Engineering
Ben-Gurion University, Beer-Sheva 84105
Email: kalmans@menix.bgu.ac.il

Spiral grain in trees is the phenomenon in which the grain direction, rather than being parallel to the tree axis, proceeds in a helical pattern along the length of the trunk. When boards are cut from such a tree log (saw cuts are necessarily parallel to tree axis) the result is a board with inclined grain. Since wood is a highly anisotropic material this results in severe degradation of mechanical function. For instance the bending strength of a board with the wood grain inclined at 20º to the longitudinal direction may be reduced by 50% or more. "Spiral grain is a very common *defect* in a tree and when excessive renders the timber valueless for use except in the round." (Record, 1914). The word *defect* (my emphasis in the previous sentence) requires some consideration. Humans exploit trees to extract structural elements; for *us* spiral grain is a defect. But we must consider also the living tree's point of view; maybe the tree doesn't mind being chiral, maybe he/she/it even finds it advantageous. Unfortunately we cannot ask the tree.

All aspects of this subject have been the object of research for centuries. Is the phenomenon genetic or is it environmental? What global influences on the tree may cause or exacerbate its development? What is the internal mechanism at the cell level causing this phenomenon? How can it be reliably detected in the standing tree? What are the implications when using the wood? Most of the above questions were already considered by Theophrastus (1916) over 2000 years ago. In the past century hundreds of research papers have dealt with the various aspects of these issues. Since more and more commercial timber is plantation grown foresters have sought guidance as to genetic and management strategies which are appropriate for spiral grain reduction/elimination. Currently it is widely accepted that the causative factor in terms of the events taking place in the cambial zone during wood formation is that during anticlinal (multiplicative) pseudotransverse cell division the slant orientation of the partition wall is preferentially (in a statistical sense) biased to the left or to the right. (See Harris (1989) for a review.) The subsequent elongation of the resulting cells at some inclination together with the plastic nature of the cambial region is said to result in a slope gradient.

The purpose of this talk is to put spiral grain into perspective. Growth stress patterns in standing trees (in the language of engineers – residual stress distributions) have been extensively investigated in the past half century using the tools of solid mechanics. (A good review can be found in Archer (1987); see also Yamamoto *et al*. (2002).) The mechanism of growth stress evolution during cell maturation is well understood. It is argued here that the development of these stresses and the formation of spiral grain are just two aspects of the same process occurring throughout the cambial zone during cell maturation. These are cells which result from periclinal (additive) cell division. A model is presented to justify this claim which is in accordance with reported patterns of growth stress and spiral grain in conifers. It therefore follows that all the parameters, whether genetically or environmentally determined, which influence growth stress must be taken into account when trying to understand the occurrence of spiral grain and, of course, if means are to be found to reduce this defect. The influence of the various physical parameters of the maturing fusiform cells is discussed and their effect on the severity of spiral grain development is considered. It is concluded that the observed preferential cell plate orientation following anticlinal division is *not* the cause of spiral grain, but is itself rather *caused by* the state of stress in the cambial zone through a mechanotransductive mechanism.

The emphasis in this talk is on the botanical background, the issues involved, and the implications of the model. Detailed mechanical analysis can be found in Schulgasser and Witztum (2007).

References

Archer, R.R. (1987). Growth Stresses and Strains in Trees. Springer. [1]

Harris, J.M. (1989). Spiral Grain and Wave Phenomena in Wood Formation. Springer. [2]

Record, S.J. (1914). The Mechanical Properties of Wood. Wiley. [3]

Schulgasser, K. & Witztum, A. (2007). The mechanism of spiral grain formation in trees. *Wood Science and Technology* **41**, 133-156. [4]

Theophrastus (1916). Enquiry into Plants, Book V (trans. A. Hort), Harvard University Press. [5]

Yamamoto, H., Kojima, Y., Okuyama, T, Abasolo, W.P. & Gril, J. (2002) Origin of the biomechanical properties of wood related to the fine structure of the multi-layered cell wall. *Journal of Biomechanical Engineering* **124**, 432-440. [6]

Soft neutral elastic inhomogeneities with membrane-type interface conditions

Y Benveniste and T Miloh

School of Mechanical Engineering
Faculty of Engineering, Tel-Aviv University, Ramat-Aviv, Tel-Aviv, 69978 Israel
Email: benben@eng.tau.ac.il

A foreign body, called an "inhomogeneity", when introduced in a host solid disturbs the stress field which is present in it . One can explore modifying the contact mechanism between the inhomogeneity and the host body so as to leave the stress field in the host solid undisturbed. If this procedure succeeds, then the inhomogeneity is called "neutral". Modification of the contact mechanism between the inhomogeneity and the host solid can be achieved by a suitably designed thick or thin interphase between them. When the interphase is thin, it can be represented by an "imperfect interface" model. In the present study we consider inhomogeneities which are softer than the host body. A "membrane-type interface" which models a thin and stiff interphase is used in rendering the inhomogeneity neutral. Examples are given for cylindrical neutral inhomogeneities of elliptical cross section under a triaxial loading, and spheroidal inhomogeneities under an axisymmetric loading.

Patient-specific simulation of the proximal femur's mechanical response validated by experimental observations

N Trabelsi*, Z Yosibash*, S Gruntman#, Y Alon# and C Milgrom&

* *Dept. of Mechanical Engineering, Ben-Gurion University of the Negev, Beer-Sheva, 84105, Israel*
#*Nuclear Research Center Negev, Israel*
& *Dept. of Orthopedics, Hadassah Medical Center, Ein-Kerem, Jerusalem*
Corresponding author's E-mail: nirtr@bgu.ac.il

Accurate methods for predicting and monitoring patient-specific bone strength are of major importance in clinical applications but are nowadays very restricted. Numerous studies address the generation of the femur's 3D model based on quantitative computerized tomography (QCT) scans with reasonable accuracy (but not satisfactory for clinical application). Herein semi-automatic algorithms applied to QCT scans in conjunction with high-order finite element (p-FE) methods show to provide excellent results when correlated to in-vitro experimental observations performed on fresh-frozen bones.

In the new approach bone's geometry is represented by smooth surfaces accurately and the inhomogeneous elastic properties are evaluated according to a similar volume as the test specimens used for their estimation. For that purpose, the QCT data were processed following several steps, starting from bone borders detection at each CT slice, trough surface approximation, to solid body representation, and finally to FE mesh generation (Figure 1).

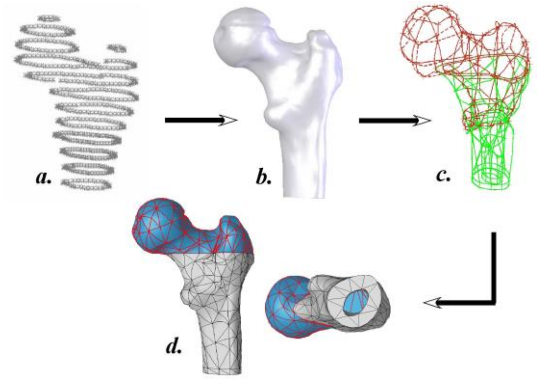

Fig. 1 The steps for generating the p-FE model: a. outer surface border points; b. approximated smooth surface; c. solid body having a cortical/trabecular separating surface; and d. meshed model with two different mesh regions.

p-FEs are used because of their many advantages over conventional h-FEs: accurate surface representation, faster numerical convergence rates achieved by increasing the polynomial degree p of the shape functions over same mesh thus controlling numerical errors easily. Also, the inhomogeneous Young's modulus (E) can be described as a spatial inhomogeneous function within the model and elements may have large aspect ratios (required in cortical regions being thin and long) and may be far more distorted.
An internal smooth surface is used to separate the cortical and trabecular regions. Within each region (cortical or trabecular) the QCT Housefeld Unit (HU) values are recalculated using a moving average method and inhomogeneous mechanical properties are assigned by LMS approximations using $E(HU)$ relations.
To validate the simulation results we performed mechanical in-vitro experiments on two freshly frozen proximal femurs at three different inclination angles, measuring head deflection and strains at several points. In Figure 2 we present one of the bones tested with the location of the strain-gauges.

The QCT scans were used to generate p-FE models of the two bones, and the FE results were compared to the in-vitro experiments. We compared the strains at the various locations on the surface and the displacements of the femur's head with these observed in the experiment. Excellent correspondence was obtained between computed and measured strains and displacements. In Figure 3 we plot the strains and displacements computed by the FE model vs. the ones measured in the experiments. We performed a linear regression which results in a slope of the regression line of about 1.03 (very close to one) and linear regression coefficient $R^2 = 0.965$ (the intercept is in percentage close to zero), see for details [1,2].

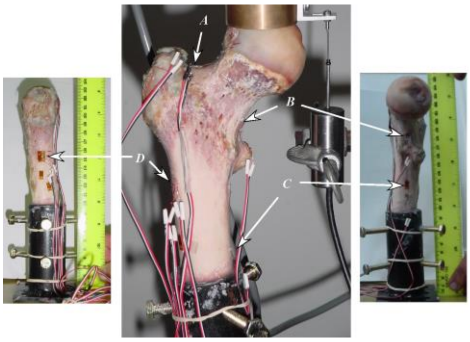

Fig. 2 Typical test and strain gauges locations: A. neck superior, B. neck inferior, C. shaft medial, and D. shaft lateral

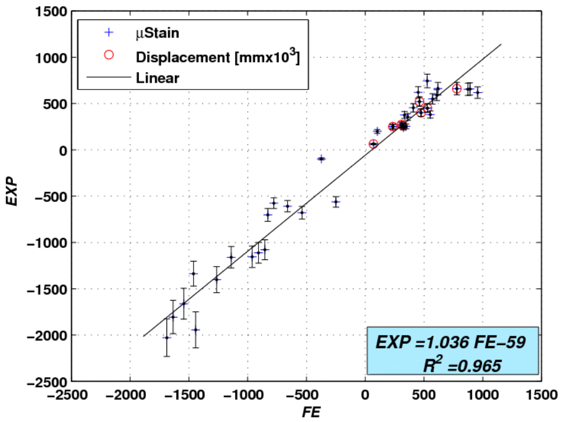

Fig. 3 Linear regression of predicted vs. measured displacements and strains (n=42)

Summary

Semi-automatic procedures for the construction of patient-specific p-FE models (from QCT scans) with distinct trabecular and cortical sub-domains and inhomogeneous Young's moduli are shown to provide very accurate results. Both displacements and strains are predicted in the same range of accuracy as the experimental errors, significantly better than any of the previous publications known to the authors. The entire simulation process requires a couple of hours, including model verification and results inspection (and can be shortened significantly to less than an hour by introducing further automatic procedures), making it suitable for clinical routinely application.

Keywords: *Proximal femur, Finite element analysis, p-FEM, Computed tomography, Bone biomechanics.*

Acknowledgements

The authors wish to thank Dr. Arie Bussiba for the help with bone experiments and Mr. Ilan Gilad for his help with experiments and FE analysis.

References

[1] Z. Yosibash, R. Padan, L. Joskowicz & C .Milgrom, "A CT-based high-order finite element analysis of the human proximal femur compared to in-vitro experiments", *J. Biomechanical Engrg*, **129**(3):297-309, 2007.

[2] Z. Yosibash, N. Trabelsi & C. Milgrom, "Reliable simulations of the human proximal femur by high-order finite element analysis validated by experimental observations", *J. of Biomechanics* (in press).

Shock tube study of the drag coefficient of a sphere

G Jourdan[1], L Houas[1], O Igra[2].

[1]Polytech' Marseille, Département de Méchanique Energétique, IUST, Université de Provence, Marseille, France
[2] The Pearlstone Center for Aeronautical Engineering Studies, Dept. of Mechanical Engineering, Ben Gurion University, Beer Sheva, Israel
Email: ozer@bgumail.bgu.ac.il

The drag acting on a sphere in a steady flow was thoroughly investigated during the past century. It resulted in detailed and accurate knowledge for the drag coefficient of a sphere in a very large range of Reynolds numbers known as the "Standard Drag Curve". However, in many engineering applications the sphere(s) motion through the fluid in which it is immersed is not steady; i.e., it experiences acceleration or deceleration. For example in nozzle flow of a solid propellant rocket, flows behind shock/blast waves propagating into a dusty gas, volcanic eruptions etc. Using the standard drag curve for such flows is, at least, questionable. For having a reliable simulation of a nonstationary two phase flow (solid particles immersed in a gaseous medium), an accurate knowledge of the particle drag coefficient is essential.

A shock tube is an ideal facility for studying the drag coefficient of a sphere in a truly non-stationary flow. Spherical particle(s) placed in a shock tube will experience large acceleration upon their interaction with the incident shock wave. This large initial acceleration will steadily decrease with increase in the particle(s) velocity until zero acceleration when (and if) the particle(s) reach the post-shock flow velocity.

Measurements of sphere drag coefficients for nonstationary flows were conducted during the past four decades. However, most of these experiments were done in a very narrow range of Reynolds numbers and most if not all of these works were done in a subsonic post-shock flows.

In the present work the drag coefficient of a sphere placed in a non-stationary flow is studied experimentally over a wide range of Reynolds numbers and in a sub and supersonic flows. Experiments were conducted in a shock tube where the investigated balls where hung far from all the tube walls, on very thin wires taken from a spider-web. During each experiment many shadowgraph photos were taken enabling an accurate construction of the sphere's trajectory. Based on the sphere's trajectory its drag coefficient was evaluated. It was shown that large difference exists between the sphere drag coefficient in a steady and non-steady flows. In the investigated range of Reynolds numbers the difference exceeds 50%. Based on the obtained results correlations for the non-stationary drag coefficient of a sphere are given. These can safely be used in two phase flows of small spherical particles immersed in a gaseous medium. A summary of the obtained results is given in the following figure.

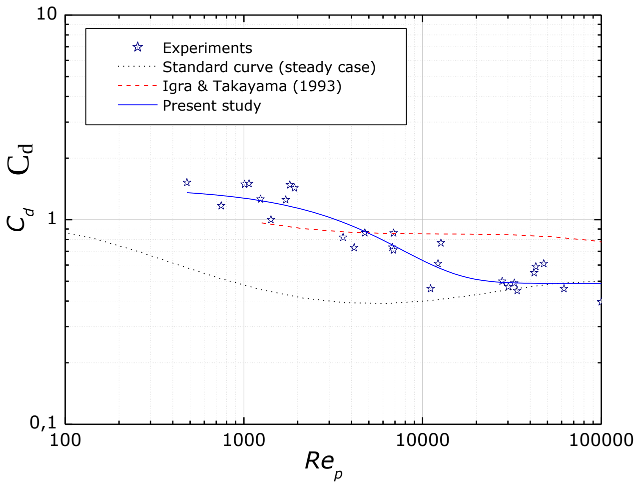

Effects of straight-walled constrictions on flow in shallow micro-channels

A. Gat, I. Frankel and D. Weihs

Faculty of Aerospace Engineering, Technion - Israel Institute of Technology
Haifa 32000, Israel. Email: gat@tx.technion.ac.il

With the advent of micro-fabrication technology micro-fluidics has become relevant to a rapidly growing spectrum of applications. Many of these applications (e.g. flow control, cooling in micro-electronic systems, etc.) involve gas flows through micro-configurations (Ho & Tai 1998). Most of the research in micro-fluidic systems has so far focused on straight and uniform channels which constitute the simplest geometrical configuration while representing a basic element in practically all applications.

We study the viscous compressible flow through micro-channels of non-uniform cross section. A lubrication approximation is applied to analyze the flow through shallow configurations whose gap width is small in comparison with all other characteristic dimensions (see figure 1). Focusing on channels with a symmetric constriction we obtain the solution to the problem by means of a Schwarz-Christoffel transformation.

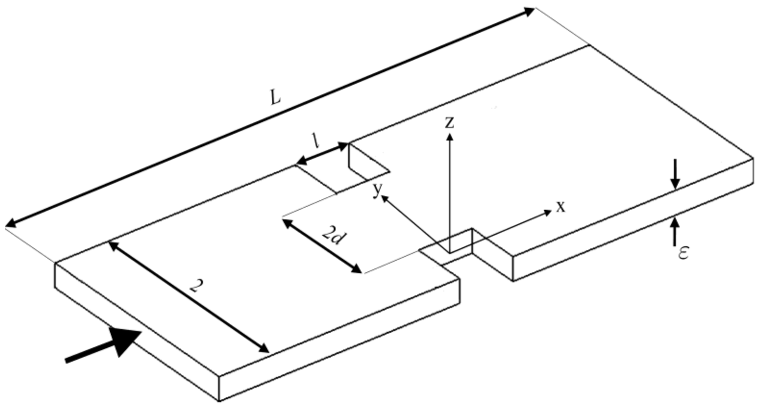

Figure 1 - A schematic view of the constricted micro-channel defining dimensions and coordinate axes (all dimensions are normalized by D, half the channel width).

From the analysis wee obtain the ratio between q and q_0 the mass-flow-rate (at given entrance and exit conditions) through constricted and uniform channel, respectively

$$\frac{q}{q_0} = \left(1 + \frac{2}{L}\Delta\right)^{-1}$$

The parameter Δ represents the mass-flow-rate losses due to constriction; Δ depends only upon the geometrical characteristics (l and d) of the constriction (see figure 1). The exact solution is obtained with the aid of elliptic-integrals (solved by numerical calculations) while asymptotic methods are used for the approximate solutions. Evidently, the explicit expression of Δ in terms of l and d is most desirable, allowing for a simple interpretation of the effects of the geometrical configuration on Δ. By use of asymptotic analysis approximation of Δ can be obtained for $d \lessapprox 1$ as a function of l and d,

$$\Delta \sim \frac{1}{2}\frac{1-d}{d}l + \frac{1}{\pi}\left[2\ln\left|\frac{1-d^2}{4d}\right| + \frac{1+d^2}{d}\ln\left|\frac{1+d}{1-d}\right|\right].$$

Thus, the first term, which is linear in l, represents the increase (for $d<1$) or reduction (for $d>1$) of the hydrodynamic resistance per unit length of an infinite straight channel resulting from changing its uniform width from unity to d. The rest of the expression on the right-hand side of the above equation, which is independent of l, represents 'end effects' associated with the transitions between the uniform channel and the constriction (or cavity) zone.

For deep cavities (*d>>1*) the following expression is obtained:

$$\Delta = \frac{1}{\pi}\ln\left(\frac{l^2+4}{4}\right) - l\left\{\frac{1}{2} - \frac{1}{\pi}\cos^{-1}\left[\frac{l}{(l^2+4)^{\frac{1}{2}}}\right]\right\}$$

We examine the influence of *l* and *d* on Δ in figure 2. All the curves descend monotonically with *d* passing through Δ*=0* at *d=1* (i.e. a uniform channel). The variations of Δ are larger for a constriction, increasing indefinitely with diminishing gap, than for a cavity where increasing the depth cannot reduce Δ below the limit of the deep cavities approximation. Thus, for all *l≤0.3* and *d>1*, Δ is vanishingly small. Evidently, the respective effects for both constrictions and cavities become more substantial with increasing length.

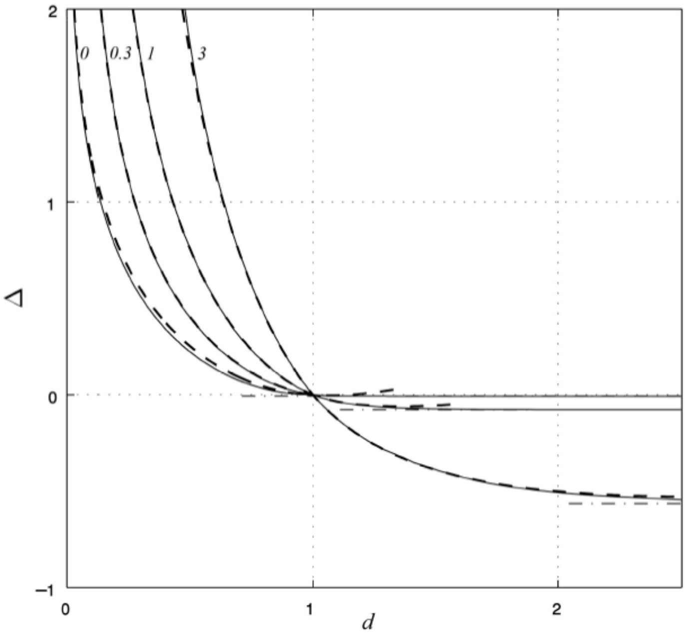

Figure 2 - *The effect of l, the constriction (cavity) length, on the variation of* Δ *with d, the gap width. Solid lines are obtained via numerical solution of the elliptic integrals. Dashed and dashed-dotted lines represent approximations for d≲1 and d>>1, respectively.*

This analytic solution was verified by examining the convergence of numerical simulations with diminishing Reynolds number and gap width. Comparison of the current results with the experimental data of Yu *et al.* (2005) reveals good agreement for the flow through micro-channels with multiple cavities.

Keywords: *Constriction, cavity, microchannel, gas flow*.

References:

Ho C.M. & Tai Y.C. 1998 Micro-electro-mechanical-systems (mems) and fluid flows. *Annu. Rev. Fluid Mech.* **30**, 579-612.

Yu, Z.T.F., Lee, Y.-K., Wong, M. & Zohar, Y. 2005 Fluid flows in microchannels with cavities. *J. Microelctromech. Syst.* **14**, pp 1386-1398.

Failure criteria for isotropic and fibrous laminated composite materials three dimensional loading case

A Rotem

Faculty of Mechanical Engineering, Technion, 32000 Haifa, Israel
Email: merar01@tx.technion.ac.il

The failure criteria are based on the separation of the stress field into two parts: isotropic and deviatoric. In addition, the failure modes of the fibrous composite materials are separated into two parts, fiber failure and matrix failure. The criterion can deal with different strengths in tension and compression (in absolute values).

For a composite, fiber failure may occur, in most cases, either by tension or compression. Tensile failure depends only on the strength of the fibers and hence on the load in the fibers direction. Compressive failure occurs as a result of micro buckling of the fibers and therefore perpendicular forces may effect the compressive strength.

The failure criterion for the matrix assumes two categories, transverse-isotropic strength and the square of the deviatoric and shear strength. It is shown that strength values from tests may be used to establish the parameters of the failure criteria.

Three-Dimensional Stress Intensity Factors for a Multicracked Spherical Pressure Vessel

M Perl[1] and V Bernstein[1]

Pearlstone Center for Aeronautical Engineering Studies
Department of Mechanical Engineering
Ben-Gurion University of the Negev
Beer-Sheva 84105, Israel
Email: merpr01@bgu.ac.il

Pressure vessels, mostly cylindrical, are widely used in many industries. However, due to their optimal specific strength (strength/weight) and their ease of packaging, spherical pressure vessels are commonly used for example as: propellant/oxidizer/pneumatic tanks on spacecrafts and aircrafts, gas tanks on LNG (liquefied natural gas) carriers, pressurized storage tanks for chemical substances, cookers for the food industry, and as metal or concrete containment structures in nuclear plants. Furthermore, whenever ***extremely high pressure*** occurs, such as in high explosion containment tanks or in the apparatus used to manufacture artificial diamonds, spherical pressure vessels are the only feasible solution. These pressure vessels are susceptible to internal cracking due to one or more of the following factors: cyclic pressurization-depressurization, repeated large temperature gradients, the presence of a heat-effected zone near a weld, corrosive agents, material degradation resulting from irradiation effects etc.

In order to assess the static fracture endurance, crack growth rate, and the total fatigue life of such a pressure vessel it is necessary to determine the prevailing mode I stress intensity factor (SIF)-K_I for one or multiple cracks. Only little attention was given so far to this problem. All the presently existing solutions by: Folias [1-2], Erdogan and Kibler [3], and Tada et al. [4], are two-dimensional, assume that the pressure vessel is a thin shell, and that the crack is a through-the-thickness crack. These solutions provide an upper limit to the SIF. In realistic situations, when one or more surface cracks emanate from the inner surface of a spherical pressure vessel of finite wall-thickness, the 2-D solutions might provide very conservative estimates for their fracture endurance and the total fatigue life.

In the present analysis a full three-dimensional analysis of a cracked spherical pressure vessel of outer to inner radius of b/a=1.1 is performed via the finite element analysis. 3-D SIFs were calculated for a wide range of crack configurations: radial cracks pertaining to arrays of n=1-20 cracks, with ellipticities of a/c=0.2, 0.5, 1.0, and 1.5 (a-crack depth, 2c-crack length), and crack-depth to wall-thickness ratios of a/t=0.025-0.8.

The obtained results clearly indicate that the SIFs are considerably affected by the three-dimensionality of the problem. In Table 1 the 3-D results for n=1 are compared to the 2-D ones provided by Erdogan and Kibler [3]. As the crack becomes shallower, and more elongated, the deviation between the 3-D SIF and the 2-D approximation increases. For very shallow and elongated cracks e.g., a/t=0.025 and a/c=0.2, which might represent the beginning of the fatigue process, the 3-D SIF is about 0.56 that of the 2-D model. Thus, crack growth rate based on the 2-D model will over estimate the realistic 3-D crack growth rate by about a factor of six, yielding a very conservative total fatigue life estimate.

Table 1: The ratio between the 3-D SIF and the 2-D SIF $\mathbf{K_I^{3-D} / K_I^{2-D}}$

a/t / **a/c**	**0.025**	**0.05**	**0.1**	**0.2**	**0.3**	**0.4**	**0.6**	**0.8**
0.2	**0.56**	**0.56**	**0.56**	**0.56**	**0.81**	**0.89**	**1.00**	**-**
0.5	**0.75**	**0.75**	**0.74**	**0.74**	**0.74**	**0.75**	**0.79**	**0.89**
1.0	**0.90**	**0.90**	**0.89**	**0.90**	**0.91**	**0.91**	**0.95**	**-**
1.5	**0.95**	**0.95**	**0.96**	**0.97**	**0.97**	**0.97**	**0.95**	**-**

[1] Aaron Fish Professor of Mechanical Engineering-Fracture Mechanics and graduate student, respectively

To exemplify the influence of the number of cracks in the array on the SIF, the distributions along a semi-circular crack, a/c=1.0 of depth a/t=0.6 for various crack arrays of n=1-20 cracks are presented in Fig. 1. These results as well as all the other results herein obtained accentuate the importance of the 3-D analysis and its parameters: n, a/c and a/t.

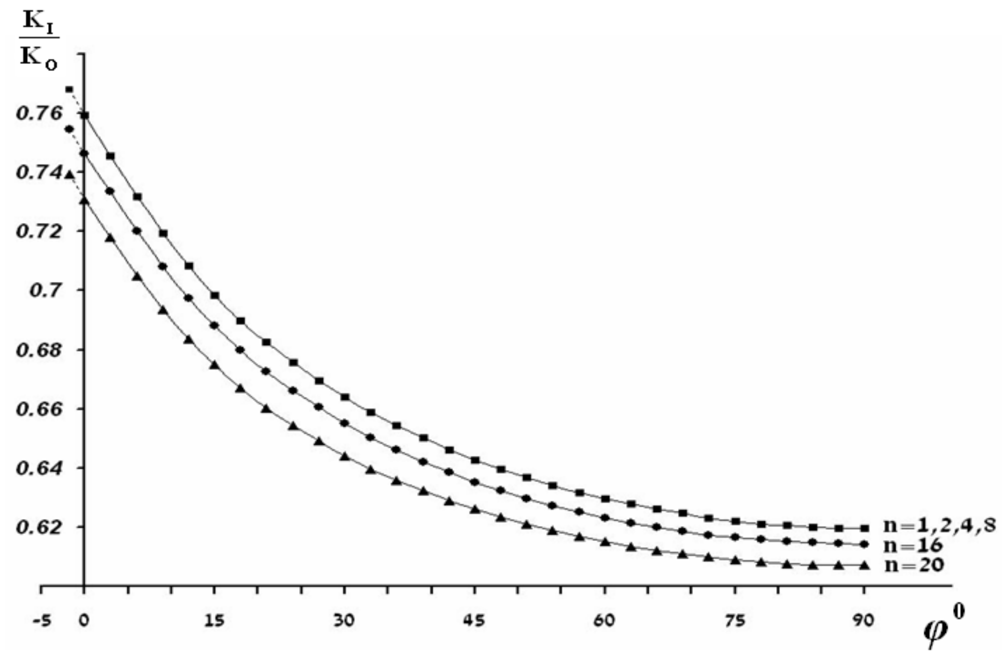

Fig. 1 K_I/K_0 variation along the crack front of a semi-circular crack

References

[1] Folias E. S., 1964, *The Stresses in a Spherical Shell Containing a Crack,* Doctoral Dissertation, California Institute of Technology.

[2] Folias E. S., 1965, "A Finite Line Crack in a Pressurized Spherical Shell," Int. J. of Fracture Mechanics, 1, pp. 20-46.

[3] Erdogan, F., and Kibler, J. J., 1969, "Cylindrical and Spherical Shells with Cracks," Int. J. of Fracture Mechanics, 5, pp. 229-237

[4] Tada, H., Paris, P. C., Irwin, G. R., 1985, *The Stress Analysis of Cracks Handbook*, 2nd Ed., Paris Productions Incorporated (and Del Research Corporation), St. Louis, MO.

Dynamic flow and failure of confined polymethylmethacrylate

D Rittel and A Brill

Faculty of Mechanical Engineering, Technion, 32000 Haifa, Israel
Email: merittel@techunix.technion.ac.il

The static and dynamic mechanical behavior of confined commercial polymethylmethacrylate (PMMA) is investigated. Cylindrical specimens are confined by means of a tightly fit metal sleeve and subjected to compression tests. The rate and pressure sensitivity of PMMA are characterized over a range of strain rates of $\dot{\varepsilon} = 10^{-3} - 10^{4}\,\mathrm{s}^{-1}$. In the quasi static regime, the material is quite ductile, exhibiting noticeable barreling. The dynamic failure mode consists of axial splitting and fragmentation at the lower strain rates $\left(\dot{\varepsilon} < 2000\,\mathrm{s}^{-1}\right)$ and confining pressures. But, at the higher strain rates and confining pressures, the failure mode changes to adiabatic shear formation of a conical plug. This failure mode transition, identified by SEM fractographic analysis, can be explained by the fact that the confinement delays the operation of damage micromechanisms, as evidenced from the post-peak slope. The response of this polymer is described using a fitted rate-dependent Drucker-Prager pressure-sensitive model, according to: $\tau_{\mathrm{flow}} = 66.78\dot{\gamma}^{0.06933} + 0.223\mathrm{p}$, for $10^{-3} \le \dot{\gamma} \le 10^{4}\,\mathrm{s}^{-1}$. This work shows that confining PMMA turns this brittle material into a ductile one, exactly like for other brittle materials such as ceramics. The present results thus fit into a general description of the pressure induced brittle-ductile transition, including rate sensitivity effects for this material.

Work output enhancement of ferromagnetic shape memory micro actuators

Y Ganor and D Shilo

Department of Mechanical Engineering, Israel Institute of Technology - Technion, Haifa 32000, ISRAEL
Email: yanivg@tx.technion.ac.il

Ferromagnetic shape memory (*FSM*) alloys are a class of materials which are both ferromagnetic and capable of undergoing a structural phase transformation. *FSM* alloys have significant advantage over conventional shape-memory temperature-based actuators because they can be remotly actuated by fast alternating magnetic fields. Therefore, *FSM* alloys attract keen attention as promising candidates for a variety of *MEMS* applications, as they can provide large strokes using small components. The most commonly used FSM alloy is Ni_2MnGa and its off-stoichiometric alloys, which are used in commercial *cm-scale FSM* actuator. However, at the current stage, no experiments of the magneto-mechnical behavior of *micro-scale* actuators were conducted.

Overall, the behavior of *FSM* alloys involves motion of twin boundaries and is significantly influenced by its microstructure. Based on a theoretical model, we have shown that down-scale specimens have finer twin boundary microstructure that consequently may increase the blocking stress characteristic such that it will enhance the output work for actuation. In light of this, a novel experimental method was realized to establish this conjecture and to provide comprehensive information on the behavior of small actuators. A series of tests demonstrated no actuation strain reduction up to extraordinary loads of 10MPa, and thus paves the route for engineering FSM high-power micro actuators by controlling their microstructure.

The electromechanical response of a double-axis electrostatic comb-drive actuator

S Yulzary and D Elata

Faculty of Mechanical Engineering, Technion - Israel Institute of Technology
Haifa 32000, Israel
Email: yulzary@tx.technion.ac.il

A novel double axis in-plane comb-drive actuator is presented in this work. In contrast to previous designs which use several single axis comb-drives, the current device uses a single comb-drive to achieve such motion. The device is activated by applying two actuation voltages. By varying these two actuation voltages a two dimensional displacement is achieved, such that the entire range of stable equilibrium displacements can be obtained.

This work focuses on the quasi-static response of the device. The displacements, which are points along the quasi-static equilibrium curves of the device, are analyzed. In addition, the electro-mechanical stability limitation, known as Pull-in, is derived. Several devices were designed and fabricated.

An experimental measurement method and system which were developed in order to measure the response of these devices are presented. This experimental system includes image acquisition and an image processing procedure. The image acquisition is synchronized with the driver which supplies actuation voltages to the device. The measured response of the devices is presented and compared to theoretical predictions. Overall, the measured results are found to be in fair agreement with the theoretical predictions (see for example Figure 1), yet some differences are observed. These differences are discussed and explained. A Finite Elements analysis is preformed, in order to evaluate the dominant non-linearity in the device response, which is caused by a Fringing Field effect.

Finally, aspects of the measurement system are described. Specifically, accuracy and repeatability of the measurements were characterized.

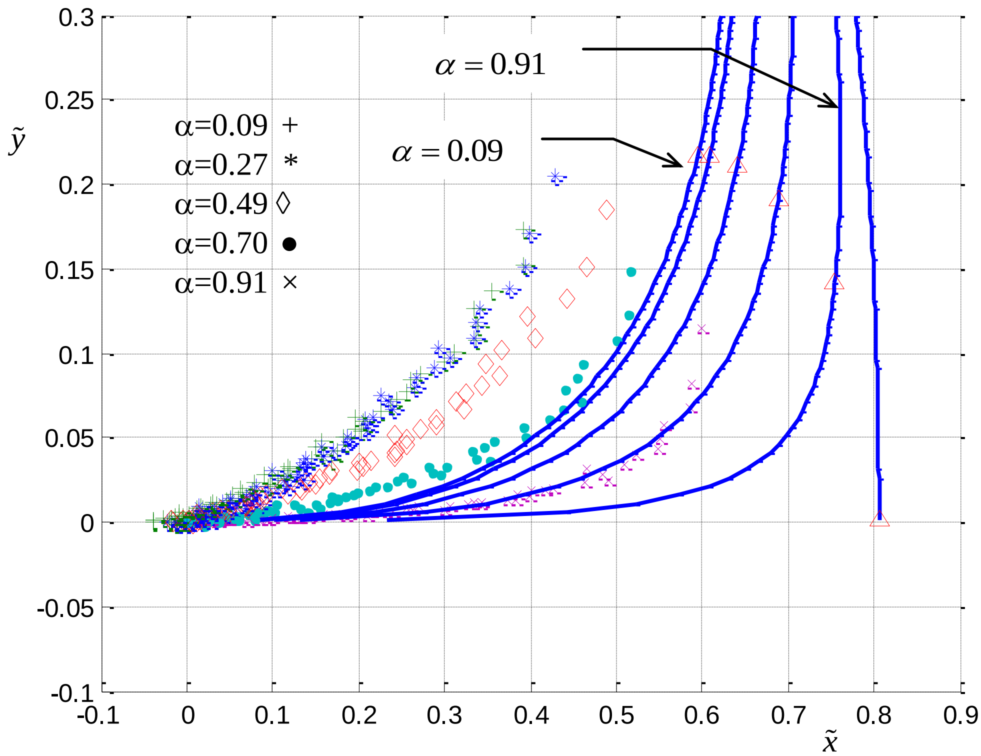

Figure 3: Theoretical (bold lines) and measured (points) equilibrium curves in the displacement domain, OL5 device. Triangles denote theoretical pull-in states. Curve α=1 was added to the theoretical curves for comparison